Soft Matter

www.rsc.org/softmatter

Volume 9 | Number 38 | 14 October 2013 | Pages 9029–9256

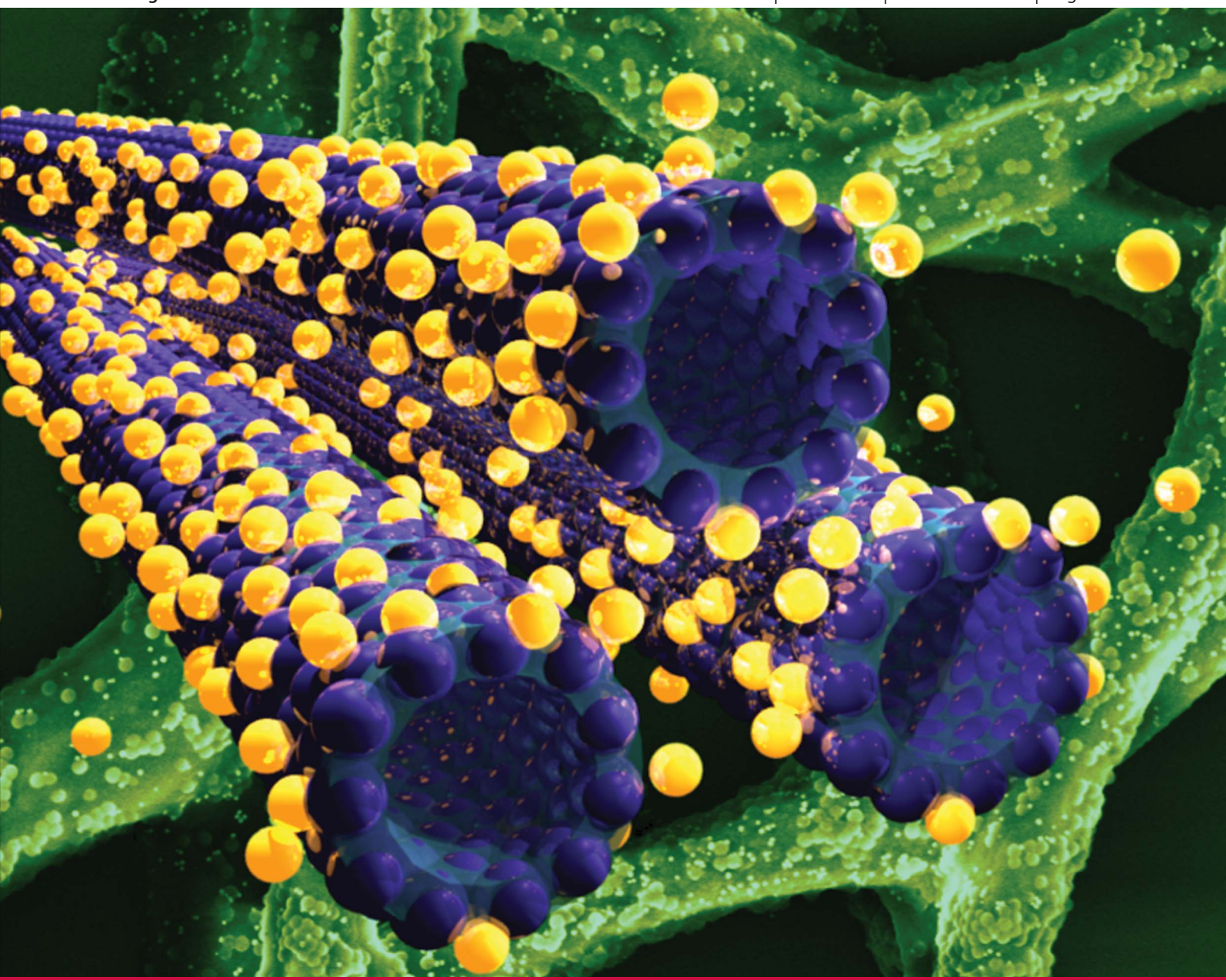

Themed issue: Directed self-assembly

ISSN 1744-683X

RSC Publishing

PAPER

Jérôme J. Crassous *et al.*

Giant hollow fiber formation through self-assembly of oppositely charged polyelectrolyte brushes and gold nanoparticles

1744-683X(2013)9:38;1-Y

Soft Matter

RSC Publishing

PAPER

View Article Online
View Journal | View Issue

Cite this: *Soft Matter*, 2013, **9**, 9111

Giant hollow fiber formation through self-assembly of oppositely charged polyelectrolyte brushes and gold nanoparticles†

Jérôme J. Crassous,*[a] Pierre-Eric Millard,[b] Adriana M. Mihut,[a] Alexander Wittemann,[c] Markus Drechsler,[d] Matthias Ballauff[ef] and Peter Schurtenberger[a]

Received 30th April 2013
Accepted 25th June 2013

DOI: 10.1039/c3sm51200b

www.rsc.org/softmatter

We report on the use of binary mixtures of oppositely charged gold nanoparticles (AuNPs) and spherical polyelectrolyte brushes (SPBs), consisting of a polystyrene core onto which long polystyrene sulfonate chains are grafted, as a simple model system to investigate the influence of directional interactions on self-assembly. We demonstrate that the mixing ratio, *i.e.*, the number of AuNPs per SPB, has a profound influence on self-assembly. In particular we report on the formation of giant hollow fibers, and present a thorough characterization of these nanostructures. We speculate that the adsorption of a few AuNPs on the SPBs appears to direct the tubular self-assembly, and discuss the analogy to the case of modified proteins such as tubulin under the action of nucleotides.

1 Introduction

Self-assembly is the key construction principle that nature uses so successfully to fabricate its molecular machinery and often highly elaborate structures. Due to their chemical, conformational and functional diversity, proteins and peptides for example have the intrinsic ability to spontaneously self-assemble into complex structures such as fibrils, shells or nanotubes, as observed for example in the formation of cytoskeletal filaments or virus assemblies.[1–5] However, their complexity represents a major limitation in our attempts to quantitatively understand their self-assembly. This motivates the use of simpler synthetic colloidal systems as functional building blocks to model association processes and to ultimately develop bioinspired applications and novel biomaterials.[4]

The association of colloids has been extensively investigated. Whereas monodisperse repulsive systems were shown to self-assemble into crystalline structures for well-defined effective volume fractions,[6] the phase diagram dramatically changes with the onset of attractive interactions.[7] Recently, the interest has been turned to the association of oppositely charged colloids, which was shown to result in new crystalline structures either in suspension,[8] which implies a fine tuning of the potential as well as a defined control of the effective volume fraction, or after adsorption on a substrate.[9,10] Moreover, the influence of the size and the number ratio in binary mixtures,[8,9] as well as the influence of an external field[11,12] have been highlighted in many studies. However, in contrast to nature's well-documented success in assembling complex structures, in colloidal self-assembly, we are still far from successfully implementing the idealized concept of a self-assembly process, where the instructions for assembly emerge from the intermolecular interactions between the building blocks.

In order to direct colloidal hierarchical assembly, one thus needs to explore new routes. As one example, so-called colloidal molecules,[13] consisting of defined dense clusters of spherical particles have already been achieved by different methods.[13–19] Nevertheless the lack of specificity in the interactions between the clusters prevents their "supramolecular" assembly. One possible approach thus is to combine the functionalities of two oppositely charged colloids in defined architectures. One could then imagine combining oppositely charged particles in one of these colloidal molecules to direct the self-assembly between the clusters. Unfortunately, at low volume fractions the mixing of oppositely charged colloids results in most cases in heteroaggregation or gelation of the dispersion with the formation of a fractal structure.[20,21]

An alternative to achieve a stable association is then to employ colloids which are radically different in size as created for example by the adsorption of cationic gold nanorods onto the surface of negatively charged microgels.[22] The adsorption of an excess of very small colloids on much larger colloids results in a charge inversion of the system, which further ensures the

[a]*Physical Chemistry, Department of Chemistry, Lund University, 221 00 Lund, Sweden. E-mail: jerome.crassous@fkem1.lu.se; Fax: +46 46222 4413; Tel: +46 46222 3677*
[b]*BASF Construction Polymers GmbH, 83308 Trostberg, Germany*
[c]*Colloid Chemistry, University of Konstanz, 78464 Konstanz, Germany*
[d]*Macromolecular Chemistry II, University of Bayreuth, 95440 Bayreuth, Germany*
[e]*Soft Matter and Functional Materials, Helmholtz-Zentrum Berlin für Materialien und Energie GmbH, 14109 Berlin, Germany*
[f]*Department of Physics, Humboldt University Berlin, 12489 Berlin, Germany*

† Electronic supplementary information (ESI) available. See DOI: 10.1039/c3sm51200b

stability of the association similarly to the intensively used layer by layer (LbL) assembly.[23] Unfortunately, this leads again to a loss of a directional interaction as a result of the association. A complementary approach is the preparation of particles with diversely functionalized hemispheres, so-called Janus particles.[24–30] As an example Janus particles with oppositely charged hemispheres were found to reorganize into defined clusters.[31] Finally, particles with heterogeneous surfaces or "patchy" particles have received considerable attention as they allow for discrete interaction sites and even specific interactions. Computer simulations illustrate the ability of these patchy particles to self-assemble into finite size clusters or well-defined structures.[32,33]

In order to direct the self-assembly of colloidal particles, we propose another approach based on the asymmetric association between two oppositely charged colloids in dilute suspensions. Only a few smaller colloids are adsorbed onto larger particles to generate local charge patches that will then induce self-assembly, similarly to patchy particles with an attractive patch, or to locally modified proteins, such as actin or tubulin under the action of nucleotides.[1,3]

We use anionic spherical polyelectrolyte brushes (SPBs), where a dense brush of polystyrene sulfonate (PSS) chains is grafted on a polystyrene (PS) core as the larger colloid. It is a well-defined system, which was intensively characterized in the past by diverse methods.[34–38] In the osmotic regime, *i.e.* at low ionic strength, the PSS chains adopt an elongated conformation, whereas at high ionic strength, in the so-called salty regime, they collapse to an overall size of about 90 nm as evidenced *in situ via* cryogenic electron microscopy.[35]

It has already been shown that proteins could be adsorbed on the SPBs.[35,39] These studies have evidenced that their strong adsorption is due to the "counterion release force", where positive patches at the surface of the proteins behave as multivalent counterions of the polyelectrolyte chains. The entropy of the entire system is increased through the concomitant release of counterions, which is the driving force of the protein immobilization. Instead of proteins, which have a complex structure and an overall radius of a few nm only, here we use adsorption of a few larger and purely cationic gold nanoparticles (AuNPs) on SPBs in order to generate hybrid complexes with a small amount of oppositely charged patches. AuNPs were selected because of their easy preparation, their strong electron contrast with respect to organic materials, and because of the sensitivity of their optical properties to their local environment.

2 Experimental

2.1 Synthesis of spherical polyelectrolyte brushes (SPBs) and gold nanoparticles (AuNPs)

SPBs were synthesized in water by photoemulsion polymerization as described in ref. 33 and 34. Long chains of poly(styrene sulfonate) were grafted to core particles made from poly(styrene) (PS) latex of 100 nm diameter. The grafting density of the brush is in the region of 0.1 nm^{-2} and the mass ratio core to shell determined gravimetrically is about 0.5. SPBs were cleansed by exhaustive ultrafiltration to remove possible traces of the free polymer in the suspension. This system has recently been directly imaged *via* cryogenic electron microscopy where the elongation of the polyelectrolyte chains in the osmotic limit as well as their collapsed state in the salty regime could be evidenced.[35] Therefore we refer to this study and the references therein for the complete characterization of this system.

Cationic AuNPs were synthesized in water as described by Niidome *et al.*[40] by $NaBH_4$ reduction of $HAuCl_4$ in the presence of 2-aminoethanethiol with a Au/$NaBH_4$/2-amino-ethanethiol ratio of 56 : 0.1 : 85 (mol%). The particles were then used for the association without further purification and the free 2-aminoethanthiol surfactant is present in the dispersion. AuNPs are monodisperse and possess a core–shell structure as evidenced by transmission electron microscopy (TEM) with a 22.7 nm radius gold core and a multilayered surfactant corona with a thickness of about 5 to 8 nm (see Fig. S1†). Further details on the characterization of this system are provided in the ESI.†

2.2 Preparation of AuNP–SPB mixtures

AuNP–SPB mixtures were prepared by slow addition of the gold suspension (0.28 g L^{-1}) at a rate of 0.25 mL min^{-1} to 16 mL dilute SPB suspensions (4×10^{-2} g L^{-1}) at 25 °C using a titrator (Titrando 809, Metrohm) equipped with a turbidity sensor ($\lambda =$ 523 nm, Spectrosense, Metrohm). Pure AuNPs were stable for approximately two weeks before sedimenting and getting adsorbed at the surface of the glass vials. Thus the characterization of pure AuNPs and the preparation of the different AuNP–SPB mixtures were done with a fresh AuNP suspension within one week.

2.3 Methods

UV spectra were recorded by a Lambda 25 spectrometer (Perkin-Elmer) at 25 °C. Zeta potential measurements were performed on a Zetasizer Nano ZS (Malvern Instruments) equipped with a He–Ne laser ($\lambda = 633$ nm). The same instrument was employed to determine the average hydrodynamic radius of the AuNPs measured in back scattering at 173°. Dynamic Light Scattering (DLS) measurements on the different mixtures were carried out at 25 °C on a light scattering goniometer setup (ALV) equipped with a He–Ne laser ($\lambda = 633$ nm) for scattering angles from 30° to 130° with an increment of 10°. Samples were highly diluted and the concentration of SPBs was set to 2.5×10^{-3} wt% in all the samples to prevent multiple scattering. The fluctuations of the scattered light were analysed with an ALV-5000 correlator.

Bright field microscopy was performed with a Leica DMRXE. A drop of the sample was deposited on a glass slide and covered with a cover slide to allow the direct imaging of the sample in the wet state. The confocal laser-scanning microscopy (CLSM) micrographs were monitored on a Leica SP5 confocal laser-scanning microscope (CLSM) operating in the inverted mode (D6000I). Samples were non-covalently dyed with Rhodamine B (5×10^{-3} g L^{-1}, excitation at 543 nm). The suspension was prepared on a glass slide with a spacer of about 200 μm.

Field-emission scanning electron microscopy (FESEM) and Scanning force microscopy (SFM) were respectively performed

using a LEO Gemini microscope equipped with a field emission cathode and a commercial SFM (Model Dimension 3100, from Veeco Instruments Inc.). Samples have been prepared by drop-casting the dilute suspensions on a silicon waver for both methods.

Transmission electron microscopy (TEM) and cryogenic transmission electron microscopy (CryoTEM) have been performed on a Zeiss EM922 EFTEM (Zeiss NTS GmbH, Oberkochen, Germany). A few microliters of the suspensions were placed on a carbon grid (Plano, 600 mesh) and the excess of liquid was removed with filter paper. CryoTEM specimens were vitrified rapidly by the method described in ref. 34.

3 Results and discussion

To achieve the formation of a few oppositely charged patches at the surface of the SPBs, a AuNP suspension (0.28 g L^{-1}) was slowly added under constant stirring to a dilute SPB suspension (4×10^{-2} g L^{-1}). A number of mixtures with different AuNP concentrations, c_{AuNP} (see inset of Fig. 1A), were prepared following the same procedure. In the rest of the study we will refer to mix 1 for the pure SPB suspension, and to mix 2 to 7 for the different mixtures with increasing amounts of AuNPs. For $c_{AuNP} \leq 4.9 \times 10^{-2}$ g L^{-1} (mix 2 to 6) the color changed from red to purple with increasing c_{AuNP} as shown in Fig. 1A, and the different mixtures remained stable for two weeks. In contrast to pure SPB suspensions, which did not show any sedimentation over months, these mixtures started to sediment for a prolonged period of time, but could easily be re-dispersed. Whereas AuNPs without SPBs became unstable after two weeks and started to aggregate and stick to the glass walls of the vials, no AuNP was getting adsorbed for these mixtures even after several months, which demonstrates the immobilization of the AuNPs as a result of their interaction with the SPBs. When $c_{AuNP} = 7.6 \times 10^{-2}$ g L^{-1} (mix 7), SPBs fully complexed with AuNPs and sedimented within an hour, resulting in a clear supernatant. Note that the slow addition of the SPBs to AuNPs resulted in suspensions that became almost immediately unstable, as it implied a large excess of AuNPs with respect to SPBs.

These direct visual observations already confirmed the strong association between the two particle species. Turbidimetric titration was performed in order to quantify the phenomenological adsorption of AuNPs on SPBs. For this purpose the optical absorbance defined as $A = -\ln(I/I_0)$, where I_0 refers to the transmitted intensity of the initial SPB suspension, was measured at $\lambda = 523$ nm as function of c_{AuNP} during the addition process (see Fig. 1A). For $c_{AuNP} < 5.6 \times 10^{-2}$ g L^{-1}, a linear dependence of A on c_{AuNP} could be observed. At $c_{AuNP} = 5.6 \times 10^{-2}$ g L^{-1}, the number ratio between AuNPs and SPBs, $N_{AuNP}/N_{SPB} \approx 2.3$, which implies that on average up to 2.3 AuNPs could be adsorbed on SPBs before the destabilization of the suspension. At higher concentrations, the absorbance strongly decreased simultaneously with a red shift of the suspension. As the detector was measuring at 523 nm, which

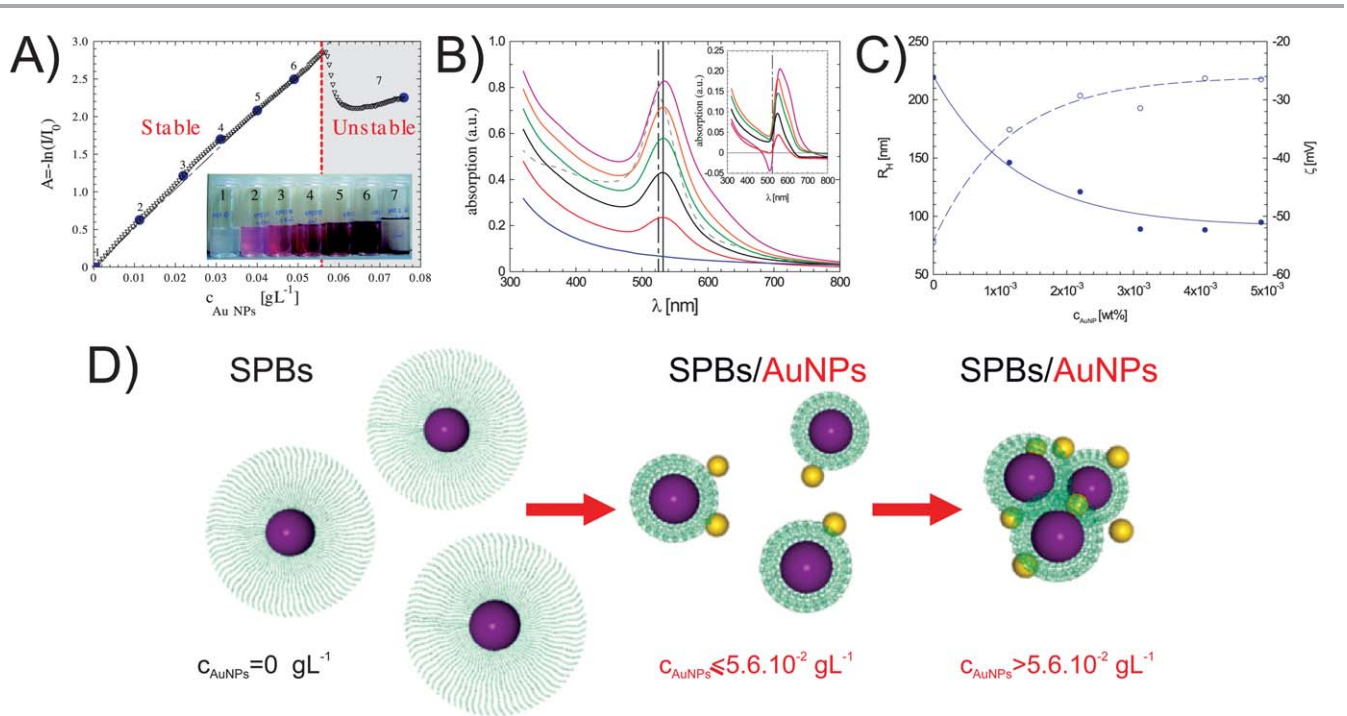

Fig. 1 (A) Turbidimetric titration of the adsorption of AuNPs on SPBs measured at $\lambda = 523$ nm. The numbers refer to the different samples presented in the inset. (B) UV spectra of AuNPs, SPBs and different AuNP–SPB mixtures (mix 2 to mix 6). The dashed line presents the absorption of a 4.9×10^{-2} g L^{-1} AuNP suspension. The full lines correspond the UV spectra of the pure 4×10^{-2} g L^{-1} SPB suspension and of the different associations (mix 2 to 6 with increasing adsorption). The inset displays the difference in absorption between the mixtures and the SPB and AuNP suspensions measured separately (see text for further explanation). (C) Hydrodynamic radius R_H (full circles) of the associated AuNPs–SPBs measured at different AuNP concentrations. The corresponding zeta potential ξ is indicated by the hollow symbols. Lines are here to guide the eyes. (D) Schematic representation of the adsorption process between SPBs and AuNPs.

was close to the plasmon absorption of AuNPs, the red shift was directly followed by a sharp decrease of the transmitted intensity. Above this concentration, the mixtures aggregated and sedimented within one hour (mix 7).

The sharp decrease in the transmission at $\lambda = 523$ nm then most likely reflects the red shift of the absorption spectrum due to this aggregation process. UV-vis absorption spectra (see Fig. 1B) were recorded for the different stable mixtures ($c_{AuNP} < 5.6 \times 10^{-2}$ g L^{-1}: mix 2 to 6) including the pure SPB (mix 1) and AuNP suspensions. Pure AuNPs had a maximum absorption at 525 nm, in good agreement with the size of the system.[41] After mixing the absorption maximum shifted to 532 nm and remained constant until $c_{AuNP} = 4.9 \times 10^{-2}$ g L^{-1} (mix 6), where it increased again to 535 nm. For each sample pure AuNP and SPB suspensions of the same concentration as in the mixture were measured separately. These two components were subtracted from the absorption of the different mixtures to probe a possible correlation between AuNPs and SPBs (see inset of Fig. 1B). An increase of the absorption followed by a red shift up to 550 nm and by a broadening of the absorption maxima to higher wavelengths were observed with increasing c_{AuNP}. We attribute this effect to changes of the local refractive index around the AuNPs and to the increasing scattering losses at low wavelength following the AuNP adsorption onto SPBs.

The AuNP-induced association was further investigated by dynamic light scattering (DLS) and electrophoretic mobility measurements (Fig. 1C). All measurements were performed approximately one week after the sample preparation. The size distributions were derived from a CONTIN analysis of the DLS measurements performed at different scattering angles (see Fig. S2†). In the early stage of the association and at low gold concentration $c_{AuNP} < 5.6 \times 10^{-2}$ g L^{-1}, the addition of AuNPs did not result in the formation of large aggregates. In contrast, the overall size was found to decrease. The hydrodynamic radius R_H attributed to SPBs and to AuNP–SPB hybrid complexes strongly evolved with increasing c_{AuNP} from 220 nm for the initial SPBs, corresponding to a fully stretched conformation of the PSS chains in the osmotic limit, to approximately 90 nm that corresponds to a collapsed SPBs in the salty regime. This analysis also confirmed the presence of free AuNPs in the suspension (see Fig. S2†). The zeta potential ξ of SPBs and AuNPs was found to be -54.5 mV and +27 mV, respectively. In the different mixtures, the addition of AuNPs resulted in the increase of ξ until a plateau was reached around -26 mV.

The evolution of R_H and ξ, as summarized in Fig. 1C, can be attributed to the adsorption of AuNPs on the surface of SPBs. In addition, an increase of the free surfactant concentration originating from the AuNP suspension, which could complex with the PSS chains, could also contribute.[37] Different microscopy methods were employed as well to probe the association of the two particles (see Fig. S3†). The different micrographs correlate with the DLS results and demonstrate the formation of AuNP–SPB clusters as well as the presence of free AuNPs. Thus, the microscopy results from dried samples provide additional evidence for the rather weak association between SPBs and AuNPs. Our findings in the early stage of the association are schematically summarized in Fig. 1D. At low AuNP concentration, AuNPs and SPBs form defined complexes and the SPB shell undergoes a transition from a stretched to collapsed configuration characterized by the decrease of the overall hydrodynamic radius. At higher concentrations the mixtures become highly unstable and rapidly form large aggregates which sediment within a couple of hours.

While the mixtures with $c_{AuNP} \leq 5.6 \times 10^{-2}$ g L^{-1} (mix 2 to 6) were stable for two weeks, we observed the formation of very long hollow fibers with an average width below 2 μm after one month as shown by SEM (Fig. 2). This finding was confirmed by optical and confocal laser-scanning microscopy (see Fig. S4 and S5†). Fig. 2B shows an SEM image of the superposition of many fibers at a higher magnification. During the drying process the fibers got more or less adsorbed to the wafer. This leads to partial or complete compression of the fibers depending upon the distance from the wafer surface. Images were taken at three distinct image planes at different heights. In the first imaged plane with the largest distance from the wafer, the fibers were still intact with an average radius R of 400 nm. In the second plane the fibers already became significantly compressed and in the third plane they appeared to be broken down and fully adsorbed on the surface of the wafer. Their widths then varied from 1.4 μm, corresponding to a compressed hollow fiber ($\approx \pi R$), to 2.7 μm characteristic for a fully adsorbed opened fiber ($\approx 2\pi R$).

A magnified fiber is shown in Fig. 2C and D. We can clearly identify both AuNPs and SPBs from their difference in size and contrast. Some individual SPBs could be observed at the surface of the fibers or partially embedded into the walls. Particles integrally incorporated into the walls could not be

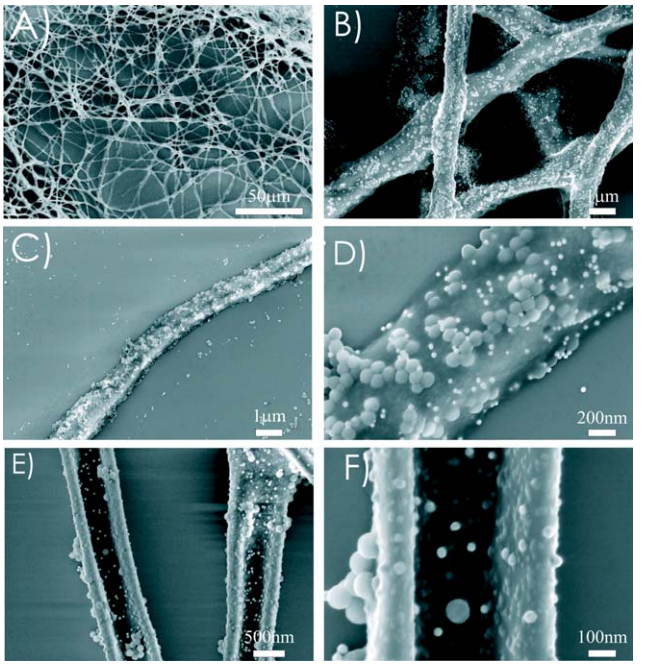

Fig. 2 SEM micrographs of hollow fibers for different aged AuNPs–SPBs mixtures, showing both a low and a high magnification: (A and B) a fibrillar network; (C and D) an individual intact fiber and (E and F) an opened fiber.

differentiated anymore, most probably as a consequence of the lack of contrast between the PS core and the PSS brush. The SEM micrographs also show the presence of open fibers (Fig. 2E and F), which allows us to estimate the wall thickness of around 160 nm. This value, of the same order as the SPB diameter measured by dynamic light scattering in the collapsed state, was confirmed by scanning force microscopy (SFM) performed on opened and closed fibers (Fig. 3).

A damaged fiber was first investigated (Fig. 3 top row). The fiber width derived from the two cross sections is around 1.2 μm, and the depression in its center can clearly be resolved. Fig. 3 validates our estimate of the thickness of the walls from the SEM analysis. Afterwards we focussed on an intact fiber. The longitudinal section (Fig. 3 middle row) confirmed the adsorption of both AuNPs and SPBs on the rather smooth surface with a well-defined height of 300 nm. The cross-sectional scan (Fig. 3 bottom row) revealed an average width around 900 nm. This value is in the order of two times higher than the width of the depression in the open fiber investigated previously, confirming the hollow character of the fibers.

Transmission electron microscopy (TEM) was then employed to get a better insight into their internal structure and composition (Fig. 4). TEM micrographs exhibit the same features as the SEM and SFM analysis, and we could image intact (Fig. 4A), collapsed (Fig. 4C), folded (Fig. 4D) and ribbon-like fibers (Fig. 4B, E and F). The TEM analysis confirms that a low number of AuNPs were present in and on the fibers. The fibers also appear surprisingly smooth on the different micrographs, and the PS core could not be distinguished in the fibers. As already observed by SEM, Fig. 4B, E and F clearly show the integration of SPBs into the fibers. This could be attributed to the polyelectrolyte chains leading to the formation of a homogeneous film and to the lack of contrast between the core and the shell of the SPBs.

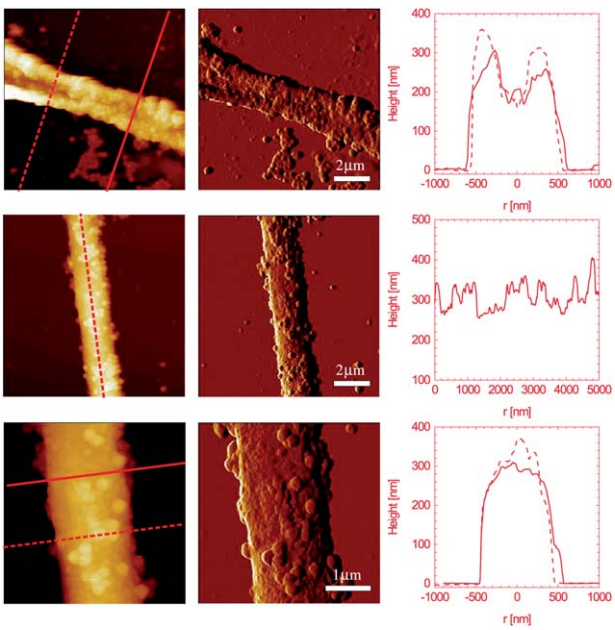

Fig. 3 SFM height and amplitude images of a damaged and an intact hollow fiber obtained for a mixture with $c_{AuNP} = 4.0 \times 10^{-2}$ g L^{-1} (mix 5). The full and dashed lines correspond to the different crosssections with their respective height profiles.

The fibers were also investigated *in situ via* cryogenic electron microscopy (CryoTEM) (see Fig. 4G and H). The same features could be observed, except that most of the fibers remained intact. Moreover the hollow character of the fibers was supported by the presence of the darker edges and was confirmed by the presence of large vesicles originating from the confined free surfactant within the fibers. The different analyses provided an overview of the structure of the fibers which can be summarized as follow: they are hollow with a diameter of about 900 nm, and the walls appear to be formed by a SPBs monolayer film with a thickness around 160 nm.

While the fibers obviously result from the self-assembly of AuNPs and SPBs, the presence of the free surfactant released after the adsorption of the AuNPs could also play a major role in this. We have thus also tried to investigate the importance of a surfactant in the fiber formation process. Different solutions consisting of SPBs and of the 2-aminoethanethiol surfactant at the same concentration as present in mix 2 to 7 were prepared. No fiber formation could be observed after 2 months in the absence of AuNPs. Moreover the same observation was made for systems that were dialyzed after the AuNP addition to remove the excess of surfactant. This indicates that the mode of association is complex and depends on the presence of all three components AuNPs, SPBs and the free surfactant, respectively. We also dissolved the gold after the nanotube formation by adding cyanide until the solutions became colorless. Even after dissolution of the gold the fibers remained intact. The fibers result from a very slow aggregation process and could be observed for various gold concentrations, nevertheless much less AuNPs than SPBs are adsorbed on the fibers. This indicates that while AuNPs are essential for the fiber formation, they are only partially incorporated. Moreover, it excludes the hypothesis of permanent discrete binding sites created by the AuNPs as a driving force for the reorganization of the SPBs into an ordered structure. Unfortunately the lack of contrast between the PS core and the PSS brush does not allow us to evidence any internal structure and local ordering in the fibers. Similarly to what is observed for instance for tubulin under the action of a nucleotide, we conclude that AuNPs seem to dynamically initiate and direct the self-assembly process as depicted in Fig. 4I.

It has been shown by Kim and Berg[42] that fractal dimensions much lower than diffusion-limited cluster aggregation (DLCA) could result from heteroaggregation of oppositely charged particles when the ionic strength is sufficiently high. The authors also suggested that sedimentation effects, when present, play a key role in the structure evolution. It is interesting to look at another intriguing self-assembly process that results in a locally 2D-structure. Geerts *et al.* recently reported the formation of "flying colloidal carpets", where polystyrene lattices coated with long DNA could form a 2D crystalline monolayer "floating" at the surface of a weakly positively charged adsorbing substrate. Under these conditions the steric stabilization ensured by DNA was found insufficient to prevent

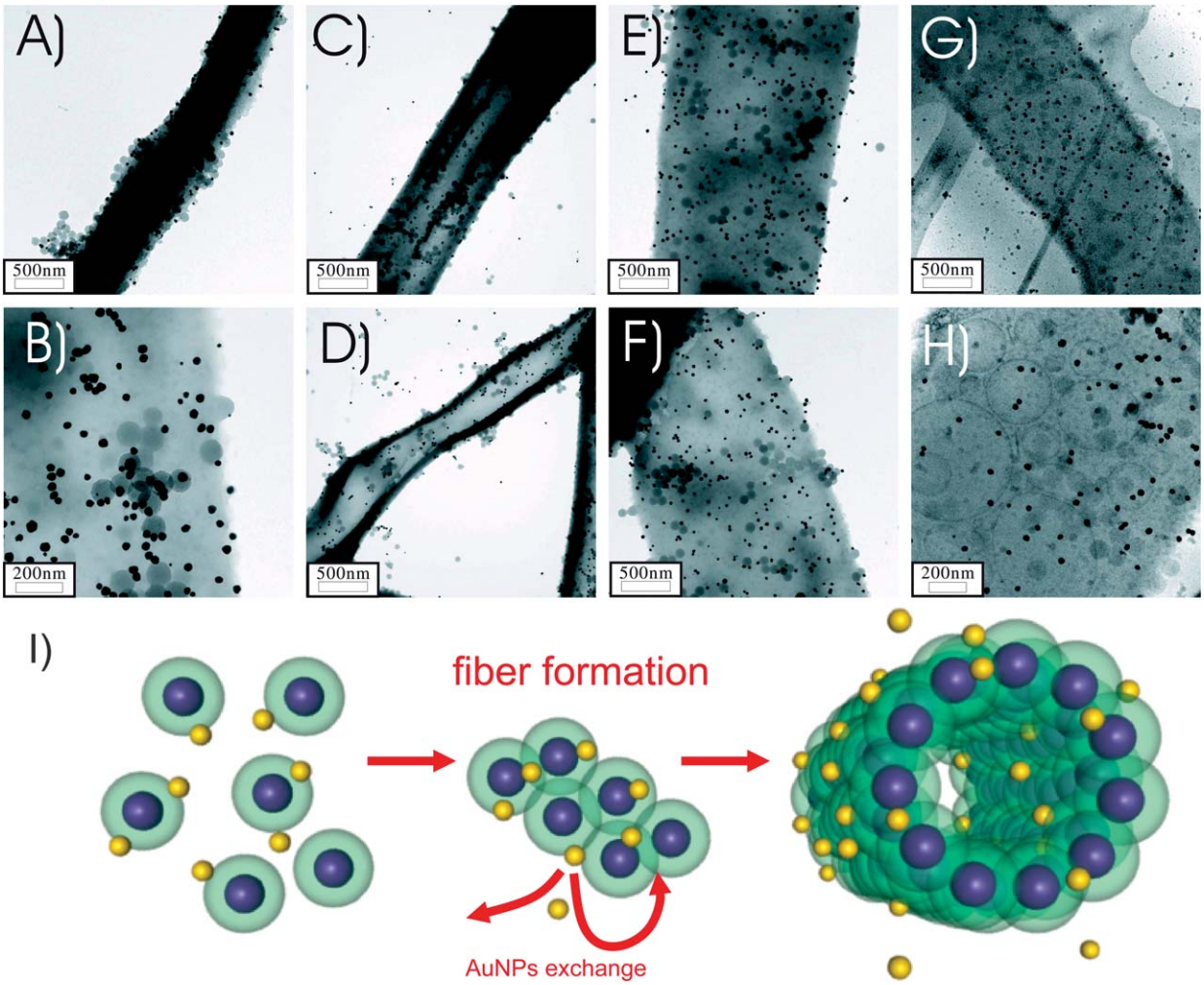

Fig. 4 (A–F) TEM micrographs of fibers with different conformations (A): intact, (C): collapsed, (B), (D), (E): opened obtained for different AuNP concentrations. (G and H) CryoTEM micrographs of an intact hollow fibers. The higher magnification (H) provides evidence for the formation of large vesicles confined into the fibers. (I) Schematic representation of the fiber formation.

the slow formation of the dense 2D crystals.[43] Therefore interactions at interfaces may as well play a major role as shown for instance for the self-assembly of cylindrical capsules using colloidal particles at fluid–fluid interfaces.[44]

In our case, the hybrid complexes sediment. Therefore, we cannot exclude a reorganization at the glass interface of the vials. In their collapsed state, the SPBs are mostly sterically stabilized as the electrostatic interaction is screened, which may explain the irreversible aggregation process and the film formation. Moreover, it was shown from simulations that patchy particles with one or two patches could self-assemble in planar structures.[43] The adsorption of a reduced number of AuNPs per SPBs then could induce the formation of these patches and direct the self-assembly of the particles, similarly to what is observed in the biological system, where the proteins have a dipolar character and self-assemble through weak and non-covalent interactions.[1,3,4]

However, while these different contributions could explain the reorganization into a locally planar structure, it could not explain the tubular self-assembly. Most reported nanotubes possess a helical chirality, where one-handedness could be realized in most cases by stereochemically impure components. Therefore the combination of components leading to non-tubular assemblies with properly chosen chiral components may give rise to nanotubes with one-handed helical chirality.[45] One possible explanation of the tubular aggregation in the AuNP–SPB mixtures could be the presence of chiral "colloidal molecules", which further rearrange with chiral or non-chiral complexes. The presence of the free surfactant, which will tend to reduce the surface energy of the monolayer could also influence the tubular formation.

In this context, it is interesting to look at the different structures formed in the present study and those observed in an earlier investigation where we looked at oppositely charged mixtures of AuNPs and core–shell polystyrene–poly(*N*-isopropylacrylamide) (PS–PNIPAM) composite microgels (CSMs).[46] For AuNP–CSM mixtures, we observed the initial formation of individual colloidal molecules, where one or few AuNPs adsorbed onto a CSM and thus formed patches, followed by the formation of finite sized clusters at higher AuNP

concentrations. Finally, at a number ratio $N_{AuNP}/N_{CSM} > 1$ the suspensions became unstable and irreversible aggregation started. However, no nanotube formation could be observed. While CSMs also have a polymeric shell where the AuNPs can adsorb, due to its crosslinked nature the ability of the particles to interpenetrate and collapse is very much reduced. Moreover, the charge density of the microgel-shell is much smaller than for the PSS brush in the SPBs. This clearly indicates the complex interplay of interactions that is required to create well-defined tubular structures through a simple self-assembly process.

4 Conclusion

This study demonstrates the interesting and unexpected possibilities to create individual three-dimensional structures such as single-walled nanotubes through a simple asymmetric self-assembly of oppositely charged colloids. However, the mode of action involved in the formation of these nanotubes is by no means clear. At first sight, the asymmetric self-assembly of differently sized and oppositely charged particles could be interpreted as the formation of hybrid building blocks with a finite number of oppositely charged patches. These could then be looked at as a simple colloidal analogue of a capsid protein in the formation of a virus shell. However, the analysis of the resulting nanotubes clearly indicates that the final number of AuNPs incorporated is smaller than the number of SPBs that form the shell of the tube. Moreover, our experiments have also indicated that the surfactant released from the AuNPs plays a vital role. Finally, a comparison between the self-assembly observed in AuNP–SPB and AuNP–CSM mixtures has added another unresolved puzzle, indicating that also the nature of the polymeric shell plays a concise role. It is, however, tempting to look at the AuNPs as a building block that initiates self-assembly only, and investigate possible analogies to the biological world where helper proteins or nucleotides play a similar role in the formation of complex biological structures.

We hope that our study will motivate further systematic investigations into the potential offered by asymmetric self-assembly, and stimulate additional experimental and theoretical works that could for example include functionalized nanoparticles with various interaction potentials.

Acknowledgements

We gratefully acknowledge financial support from the Swiss National Foundation, the Faculty of Science of Lund University and the Swedish Research Council VR through the Linnaeus Center of Excellence on Organizing Molecular Matter. AW acknowledges financial support from the Deutsche Forschungsgemeinschaft within SFB 840/B5.

References

1 A. J. Ridley and A. Hall, *Cell*, 1992, **70**, 389.
2 C. I. Branden and J. Tooze, *Introduction to Protein Structure*, Garland Science, New York, 2nd edn, 1999.
3 B. Alberts, A. Johnson, J. Lewis, M. Raff, K. Roberts and P. Walter, *Molecular Biology of the cell*, Garland, New York, 5th edn, 2008.
4 S. G. Zhang, *Nat. Biotechnol.*, 2003, **21**, 1171.
5 A. K. Das, R. Collins and R. V. Ulijn, *Small*, 2008, **4**, 279.
6 P. N. Pusey and W. van Megen, *Nature*, 1986, **320**, 340.
7 V. J. Anderson and H. N. W. Lekkerkerker, *Nature*, 2002, **416**, 811.
8 M. E. Leunissen, C. G. Christova, A. P. Hynninen, C. P. Royall, A. I. Campbell, A. Imhof, M. Dijkstra, R. van Roij and A. van Blaaderen, *Nature*, 2005, **437**, 235.
9 E. V. Shevchenko, D. V. Talapin, C. B. Murray and S. O'Brien, *J. Am. Chem. Soc.*, 2006, **128**, 3620.
10 D. Talapin, E. V. Shevchenko, C. B. Murray, A. V. Titov and P. Kral, *Nano Lett.*, 2007, **7**, 1213.
11 A. Yethiraj and A. van Blaaderen, *Nature*, 2003, **421**, 513.
12 W. D. Ristenpart, I. A. Aksay and D. A. Saville, *Phys. Rev. Lett.*, 2003, **90**, 128303.
13 A. van Blaaderen, *Science*, 2003, **301**, 470.
14 D. Zanchet, C. M. Micheel, W. J. Parak, D. Gerion, S. C. Williams and A. P. Alivisatos, *J. Phys. Chem. B*, 2002, **106**, 11758.
15 V. N. Manoharan, M. T. Elsesser and D. J. Pine, *Science*, 2003, **301**, 483.
16 S. C. Glotzer, M. J. Solomon and N. A. Kotov, *AIChE J.*, 2004, **50**, 2978.
17 E. W. Edwards, D. Wang and H. Mohwald, *Macromol. Chem. Phys.*, 2007, **208**, 439.
18 A. B. Pawar and I. Kretzschmar, *Macromol. Rapid Commun.*, 2010, **31**, 150.
19 J. M. Romo-Herrera, R. A. Alvarez-Puebla and L. M. Liz-Marzan, *Nanoscale*, 2011, **3**, 1304.
20 W. Lin, M. Kobayashi, M. Skarba, C. Mu, P. Galletto and M. Borkovec, *Langmuir*, 2006, **22**, 1038.
21 E. Sanz, M. E. Leunissen, A. Fortini, A. van Blaaderen and M. Dijkstra, *J. Phys. Chem. B*, 2008, **112**, 10861.
22 M. Karg, I. Pastoriza-Santos, J. Perez-Juste, T. Hellweg, L. M. Liz-Marzan and M. Luis, *Small*, 2007, **3**, 1222.
23 J. B. Schlenoff, H. Ly and M. Li, *J. Am. Chem. Soc.*, 1998, **120**, 7626.
24 A. Perro, S. Reculusa, S. Ravaine, E. Bourgeat-Lamic and E. Duguet, *J. Mater. Chem.*, 2005, **15**, 3745.
25 S. Berger, A. Synytska, L. Ionov, K. J. Eichhorn and M. Stamm, *Macromolecules*, 2008, **41**, 9669.
26 W. Lu, M. Chen and L. Wu, *J. Colloid Interface Sci.*, 2008, **328**, 98.
27 T. Isojima, M. Lattuada, J. B. V. Sande and T. A. Hatton, *ACS Nano*, 2008, **2**, 1799.
28 J. W. Kim, D. Lee, H. C. Shum and D. A. Weitz, *Adv. Mater.*, 2008, **20**, 3239.
29 B. Wang, B. Li, B. Zhao and C. Y. Li, *J. Am. Chem. Soc.*, 2008, **130**, 11594.
30 A. Walther and A. H. E. Muller, *Soft Matter*, 2008, **4**, 663.
31 L. Hong, A. Cacciuto, E. Luijten and S. Granick, *Nano Lett.*, 2006, **6**, 2510.
32 Z. Zhang and S. C. Glotzer, *Nano Lett.*, 2004, **4**, 1407.

33 A. Giacometti, F. Lado, J. Largo, G. Pastore and F. Sciortino, *J. Chem. Phys.*, 2010, **132**, 174110.
34 X. Guo and M. Ballauff, *Macromolecules*, 1999, **32**, 6043.
35 A. Wittemann, M. Drechsler, Y. Talmon and M. Ballauff, *J. Am. Chem. Soc.*, 2005, **127**, 9688.
36 Y. Mei, K. Lauterbach, M. Hoffmann, O. V. Borisov, M. Ballauff and A. Jusufi, *Phys. Rev. Lett.*, 2006, **97**, 158301.
37 L. Samokhina, M. Schrinner and M. Ballauff, *Langmuir*, 2007, **23**, 3615.
38 M. Ballauff, *Prog. Polym. Sci.*, 2007, **32**, 1135.
39 A. Wittemann and M. Ballauff, *Phys. Chem. Chem. Phys.*, 2006, **8**, 5269.
40 T. Niidome, K. Nakashima, H. Takashi and Y. Niidome, *Chem. Commun.*, 2004, 1978.
41 S. Link and M. A. El-Sayed, *J. Phys. Chem. B*, 1999, **103**, 4212.
42 A. Y. Kim and J. C. Berg, *J. Colloid Interface Sci.*, 2000, **229**, 607.
43 N. Geerts and E. Eiser, *Soft Matter*, 2010, **6**, 664.
44 K. V. Edmond, A. B. Schofield, M. Marquez, J. P. Rothstein and A. D. Dinsmore, *Langmuir*, 2006, **22**, 9052.
45 T. Yamamoto, T. Fukushima and T. Aida, *Adv. Polym. Sci.*, 2008, **220**, 1.
46 J. J. Crassous, P. E. Millard, A. M. Mihut, F. Polzer, M. Ballauff and P. Schurtenberger, *Soft Matter*, 2012, **8**, 1648.

